

Fingerprint Presentation Attack Detection by Channel-wise Feature Denoising

Feng Liu, Zhe Kong, Haozhe Liu, Wentian Zhang, Linlin Shen*

Abstract—Due to the diversity of attack materials, fingerprint recognition systems (AFRSs) are vulnerable to malicious attacks. It is of great importance to propose effective Fingerprint Presentation Attack Detection (PAD) methods for the safety and reliability of AFRSs. However, current PAD methods often have poor robustness under new attack materials or sensor settings. This paper thus proposes a novel Channel-wise Feature Denoising fingerprint PAD (CFD-PAD) method by considering handling the redundant “noise” information which ignored in previous works. The proposed method learned important features of fingerprint images by weighting the importance of each channel and finding those discriminative channels and “noise” channels. Then, the propagation of “noise” channels is suppressed in the feature map to reduce interference. Specifically, a PA-Adaption loss is designed to constrain the feature distribution so as to make the feature distribution of live fingerprints more aggregate and spoof fingerprints more disperse. Our experimental results evaluated on LivDet 2017 showed that our proposed CFD-PAD can achieve 2.53% ACE and 93.83% True Detection Rate when the False Detection Rate equals to 1.0% (TDR@FDR=1%) and it outperforms the best single model based methods in terms of ACE (2.53% vs. 4.56%) and TDR@FDR=1% (93.83% vs. 73.32%) significantly, which proves the effectiveness of the proposed method. Although we have achieved a comparable result compared with the state-of-the-art multiple model based method, there still achieves an increase of TDR@FDR=1% from 91.19% to 93.83% by our method. Besides, our model is simpler, lighter and, more efficient and has achieved a 74.76% reduction in time-consuming compared with the state-of-the-art multiple model based method. *Code will be publicly available.*

Index Terms—Presentation attack detection, feature denoising, convolutional neural networks, generalization, domain adaption, PA-Adaption loss

I. INTRODUCTION

In recent years, with the increasing use of mobile payment, online banking, and other applications, a large number of smart devices are growing exponentially [1–4]. Due to the security requirements, more and more smart devices tend to use Automated Fingerprint Recognition Systems for personal authentication [2]. However, AFRSs are vulnerable to malicious attacks, such as 2D or 3D artificial fingerprints made of gelatin, silicone, etc. [2, 5–9]. To ensure that the user has a secure environment against presentation attacks (PA), lots of PAD methods have been proposed to solve this problem [10, 11]. Meanwhile, to deal with the threat

and promote anti-spoofing techniques, a series of fingerprint LivDet competitions have been held since 2009 [12]. Many public datasets e.g. LivDet 2011, LivDet 2013, LivDet 2015, LivDet 2017 et.al are available to evaluate the performance of fingerprint PAD [12–14].

Generally, PAD methods can often be divided into two categories, i.e. hardware and software based approaches [11, 15]. For hardware approaches, special sensors such as imaging technologies based on multispectral, short-wave infrared and, optical coherent tomography (OCT), have been developed to extract live features like odor, blood flow and, heartbeat to discriminate the live samples from spoof samples [2, 5, 16–25]. For instance, a spectroscopy-based device proposed by Nixon et al. [21] can obtain the spectral features of the fingertip, which has been proven to effectively distinguish between spoof and live fingertip. Reddy et al. [22] used a pulse-oximetry-based device to capture the percentage of oxygen in the blood and the heart pulse rate for live detection. OCT devices were applied by Liu et al. [5] to collect depth-double-peak features and sub-single-peak features of fingerprint, which achieved 100% accuracy over four types of artificial fingerprints. Ultrasonic fingerprint sensors were used by Agassy et al. [23] to determine whether the finger is a spoof fingertip or not. Liu et al. [2] proposed a One-Class framework for PAD using OCT. As only bonafide is required for training, this method not only has better generalization ability but also alleviates the data dependence problem. However, the aforementioned methods are sensor-dependent and they require additional hardware devices such as OCT-based devices and Raspireader [24, 25]. The expensive hardware costs limit the widespread usage of these approaches.

In contrast, software-based methods work without extra hardware devices. They can also be divided into two categories: the traditional PAD methods and the CNN-based PAD methods. Traditional methods distinguish spoof from live fingerprints by extracting hand-crafted features such as anatomical features (e.g. the locations and distribution of core), physiological features (e.g. perspiration and ridge distortion), and texture based features, from the fingerprint images [26–29]. For example, encoding skin distortion information, Fractional Fourier transforms and curvelet transform-based method are all effective methods adopted to extract hand-crafted features to discriminate live and spoof fingerprints [28, 30, 31]. However, these methods are sensitive to “noise”, so they have a poor generalization performance [32]. In addition, feature generators need to be manually designed for different tasks [33].

With the development of computer vision, CNN has begun

The correspondence author is Linlin Shen and the email: llshen@szu.edu.cn

Feng Liu, Zhe Kong, Haozhe Liu, Wentian Zhang, and Linlin Shen are with the College of Computer Science and Software Engineering, Shenzhen University, Shenzhen 518060, China; SZU Branch, Shenzhen Institute of Artificial Intelligence and Robotics for Society, China; Guangdong Key Laboratory of Intelligent Information Processing, Shenzhen University, Shenzhen 518060, China.

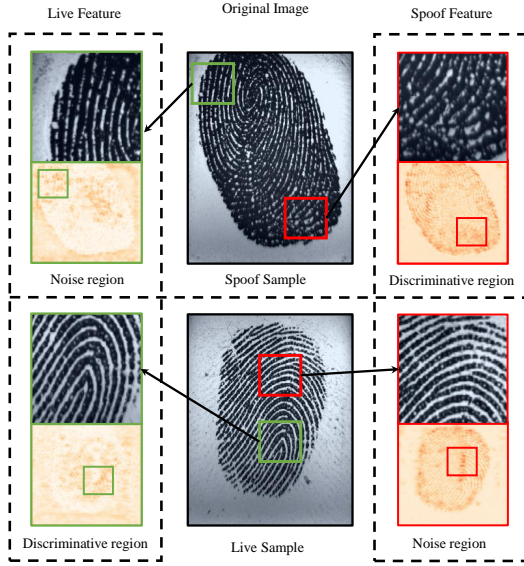


Fig. 1. The samples of live features and spoof features on fingerprint images. The images in the first row represent the spoof fingerprint and the corresponding live and spoof features. The images in the second row represent the spoof fingerprint and the corresponding live and spoof features. The second column represents the original image. The patches in the green box represent the live features of the original image and the patches in the red box represent the spoof features of the original image.

to be widely used in fingerprint PAD. CNN-based methods are learning-based and the convolutional layer with pooling layer in CNN can automatically extract features of different scales. Compared with traditional methods, CNN-based methods reduce human intervention and make feature extraction simple because there is no need to manually design feature generators for specific tasks [33]. CNN-based methods outperform the solutions using hand-crafted features by a wide margin [1, 13, 33, 34]. Typically, Nogueira et al. [33] pre-train deep CNNs for the task of object recognition and then fine-tune the CNN for fingerprint PAD. This is a global based method and the input of the network is the whole image. VGG and AlexNet have been successfully applied for fingerprint PAD via transfer learning, which achieved better results than randomly initialized weights in LivDet 2015 [13]. Chugh et al. [1] proposed a deep convolutional neural network based method. In their method, they utilized fingerprint prior knowledge by extracting local patches centered and aligned using minutiae to train the MobileNet-v1 CNN model. The above-mentioned methods improved the performance of fingerprint PAD, but they also raise new problems. One of the major limitations of the above two methods is their poor generalization performance against sensors that are unknown during training. Both of the two methods achieved good accuracy when the sensors of the training set and the testing set are the same. However, they did not get a good performance when the sensors in the training set and testing set are different. In the method proposed by Nogueira et al. [33], the Average Classification Error (ACE) is as high as 25.28% when the type of sensor used for testing

is different from the one used in training. Similarly, in the method proposed by Chugh et al. [1], the ACE is higher than 25% when the training set is Biometrika 2011 and the testing set is ItalData 2011 or vice versa.

In order to improve the poor generalization performance against different sensors, Chugh et al. [35] proposed a novel style-transfer based method to improve both the cross-material and cross-sensor generalization performance of fingerprint PAD. They transferred the style characteristics between fingerprint images of known materials with the goal of synthesizing fingerprint images corresponding to unknown materials. In this method, they leveraged centered and aligned minutiae-based prior knowledge to propose a style-transfer-based wrapper, which is used to transfer the style characteristics of known fingerprint materials. And then the CNN was supervised to learn generative-noise invariant features to improve the generalization performance. This method based on data augmentation, which increased the ACE of Slim-ResCNN and FSB from 94.01%, 95.44% to 95.37%, 95.88%, respectively [1, 35, 36]. Although this method had improved the average cross-sensor spoof detection performance, it needs images from the target material or target sensor to synthesize new images, which may not be accessible [32]. Meanwhile, they used patches as input to synthesis style-transferred data. Using patches as input not only leads to the information loss of other regions but also the relative spatial position.

Subsequently, Liu et al. [32] proposed a global-local model based PAD method to overcome the above-mentioned limitations to some extent. In this method, no images of target material or target sensor appear in the training set, and they proposed a rethinking module to connect a global and a local module. The final spoof score is calculated by averaging the global and local spoof scores. This method achieved an average classification error of 2.28% in cross-sensor settings. However, this method is based on ensemble learning, which uses two models for training and finally combines the two models by calculating the average score. This multi-model method requires the integration of multiple models and makes training complicated and time-consuming at the same time. Algorithms achieving good performance using global-local features may not be suitable for deployment conditions where the decision needs to be made quickly. Meanwhile, this method also used the heat maps in the local module and found that there exist some discriminative regions for PAD, but they did not explore further about this phenomenon.

Based on the above considerations, we further analyzed the essence of the deep learning based method for fingerprint PAD and found an interesting phenomenon. Regardless of whether the input fingerprint images are live or spoof, they contain both live and spoof features when the network makes predictions for fingerprint PAD. Grad-CAM [37] is used to locate the regions of interest and visualize the heat map in a fingerprint image. The features which can activate the heat map in a fingerprint image can be called live features. And then we reverse the heat map and now we call those features which can activate the reversed heat map spoof features. Correspondingly, we deem

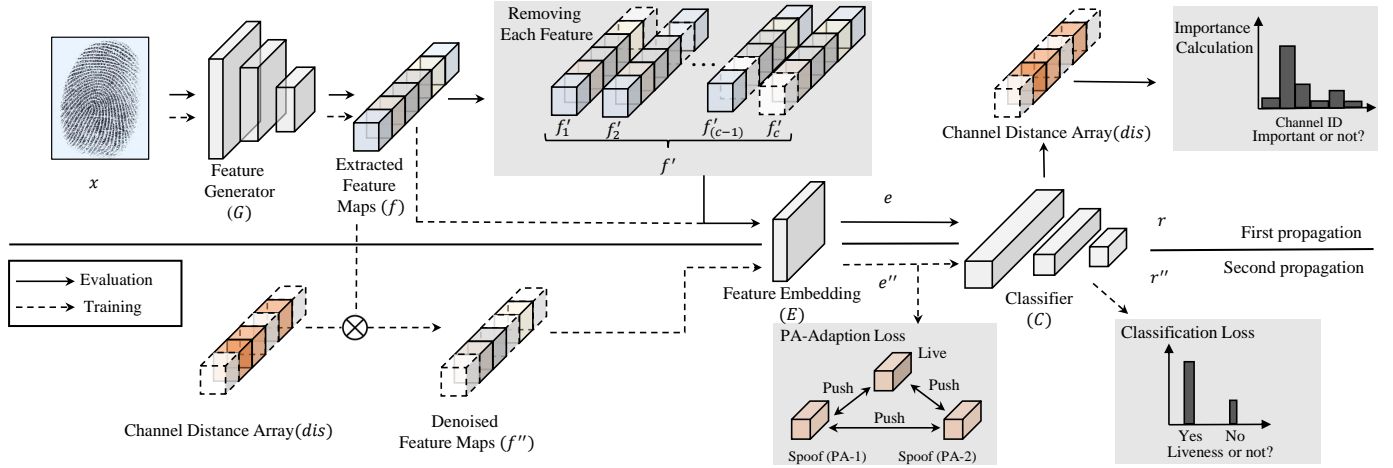


Fig. 2. An overview of the proposed fingerprint PAD method(CFD-PAD) based on channel-wise denoising.

the patches which have the same labels with original images as discriminative regions while the patches that have different labels with original images can be regarded as "noise" regions. As shown in Fig 1, whether the original image is a live sample or spoof sample, it contains abundant live and spoof features. The patches framed by the green line are live features and the patches framed by the red line are spoof features. If the input sample is a live image, the discriminative regions contain a lot of live features while the "noise" regions contain a lot of spoof features. In contrast, the discriminative regions contain a lot of spoof features while the "noise" regions contain a lot of live features if the input sample is a spoof fingerprint image. Whether it is a live image or a spoof image, the discriminative regions and "noise" regions exist in one fingerprint image simultaneously, which proves that there exists a lot of "noise" in a fingerprint image. For one original image, when the network utilizes some features to make predictions, there exist some "noises" that may interfere with the network. The same situation appears in the channels of a feature map. The feature map contains a large number of feature channels and also contains a large number of "noise" channels. Thus, we propose a novel fingerprint PAD method based on channel-wise feature denoising in this paper.

Feature denoising is a common method in computer vision. Traditional denoising methods often denoise through image analysis and modeling [38]. Many classic methods such as anisotropic diffusion, total variation denoising et.al, use hand-engineered algorithms to recover a clean signal from noise input under the assumption that both signal and noise exhibit particular statistical regularities [38–41]. The traditional denoising method is simple and effective but the parametric models limited their capacity and expressiveness [38]. However, the essence of the current feature denoising in the deep learning based method is to suppress the "noise" in the feature map to make the responses focus on visually meaningful regions [42]. For instance, in the field of adversarial attack, Xie et al. [42] found that adversarial perturbations on images lead to "noise" in the features constructed by convolutional

networks. Thus, they developed new network architectures that increase adversarial robustness by performing feature denoising. Specifically, the networks contain blocks that denoise the features using non-local means or other filters. The feature denoising networks substantially improve the adversarial robustness in both white-box and black-box attack settings. Similar to feature denoising, attention is another field in computer vision [43–47]. The attention model tends to focus selectively on some important parts of the image while ignoring other irrelevant parts[46, 47]. Fu et al. [45] proposed a novel Dual Attention Network (DANet) with a self-attention mechanism to enhance the discriminant ability of feature representations for scene segmentation. The aforementioned studies show that the denoising strategy is crucial for computer vision and has already been applied in different tasks successfully. However, the utilization of denoising strategy in the classification task, especially in PAD has rarely been discussed.

In this paper, for the time first, we to employ the denoising strategy to improve the generalization ability of fingerprint PAD. Fig. 2 shows the flowchart of the proposed method. The training stage contains three parts: a) extracting "noise" channels from feature maps, b) suppressing those selected "noise" channels in the feature maps to avoid interference, c) designing PA-Adaption loss to align the feature domain of fingerprint. Given an input image, the model firstly evaluates the importance of each channel in the feature map to find those "noise" channels. Those "noise" channels correspond to "noise" regions with abundant "noise" features. And then we minimize the interference of "noise" regions by suppressing the "noise" channels. Finally, to alter the feature distribution of different sensors of different materials, we design a PA-Adaption loss to align the feature domain of fingerprint by pulling all the live fingerprints close but pushing the spoof ones of different materials or sensors apart. In this paper, we propose a novel fingerprint PAD method based on channel-wise feature denoising. Unlike other methods, we are the first to propose the "noise" regions in fingerprint PAD. We successfully found those channels that correspond to "noise"

regions and remove the interference of these "noise" completely. Experimental results show that the proposed method is efficient and time-saving, which can significantly improve the performance of PAD, and outperform the state-of-the-art methods in cross-sensor and cross-material settings.

The main contributions of this paper are summarized as follows.

- A channel-wise feature denoising model is first proposed for fingerprint PAD in this paper. By filtering the redundant information or "noise" regions on the feature map, the fingerprint PAD performance can be significantly improved.
- An effective method to evaluate each channel and suppress the propagation of "noise" channels is proposed. By weighting the importance of each channel, "noise" channels can be suppressed.
- A new loss function that alters the feature distribution of different sensors or different materials is designed. A PA-Adaption loss is designed to align the feature domain of fingerprint by pulling all the live fingerprints close while pushing the spoof ones of different materials or sensors apart.
- Experimental results carried on LivDet 2017 show that the proposed CFD-PAD can achieve an Average Classification Error (ACE) of 2.53% and a True Detection Rate (TDR) of 93.83% when the False Detection Rate (FDR) equals to 1.0% in the case of cross-material. In the case of cross-sensor, our proposed method achieves 19.80% ACE and 32.32% True Detection Rate when the False Detection Rate equals to 1.0%. Meanwhile, our method is based on a single lightweight model, which is time-saving and suitable for deployment conditions.

II. PROPOSED APPROACH

As the overview shown in Fig. 2, our method, denoted as CFD-PAD, applies a channel-wise denoising model for PAD. The proposed method includes three stages in the training process, i.e., evaluating the importance of each channel, suppressing the propagation of "noise" channels, and aligning channel-wise domains. In the first stage, a channel distance array is generated to measure the importance of each channel in the feature map. In the second stage, we use the channel distance array to suppress the propagation of the "noise" channels. In the last stage, PA-Adaption loss is employed to push the samples apart from all samples of different materials or sensors. In this section, we first gave the system framework of the proposed method and then detailly introduced these three stages one by one.

A. System Framework

To better describe our method, we first set up the basic notations used in this paper: (x, y) denotes a data sample, x is an input image and the corresponding label is y . $G(\cdot)$ denotes the feature generator module, $E(\cdot)$ denotes the feature embedding module, $C(\cdot)$ denotes the classifier and θ_g , θ_e , θ_c are their parameters respectively. We use f to denote the

Algorithm 1 Channel-wise Feature Denoising PAD Method (CFD-PAD)

Input:

Training Set of Images: $X_{train}=\{x_1, \dots, x_i, \dots, x_n\}$;
 Groundtruth of X_{train} : $Y_{train}=\{y_1, \dots, y_i, \dots, y_n\}$;
 Attack type of X_{train} : $A_{train}=\{a_1, \dots, a_i, \dots, a_n\}$;
 Feature Generator: $G(\cdot)$ with learning parameters θ_g ;
 Feature Embedding: $E(\cdot)$ with learning parameters θ_e ;
 Classifier: $C(\cdot)$ with learning parameters θ_c ;
 Loss Function: Cross-entropy Loss function $\mathcal{L}_c(\cdot, \cdot)$ and PA-Adaption Loss function $\mathcal{L}_t(\cdot, \cdot)$;
 Training Epoch Number: e ;
 Learning Rate: α ;
 Channel's number of g_t : c
 channel distance array: dis

Output:

- 1: Initialize θ_g , θ_e , θ_c from the model pretrained on ImageNet.
- 2: Set all the values in array dis to 0
- 3: **for** $j = 1$ to e **do**
- 4: **for** $x \in X_{train}$ **do**
- 5: $f \leftarrow G(x)$;
- 6: $e \leftarrow E(f)$;
- 7: $o \leftarrow C(e)$;
- 8: $r \leftarrow softmax(o)$;
- 9: // Evaluate the importance of each channel
- 10: **for** $i = 1$ to c **do**
- 11: $f'_i \leftarrow$ Suppress the i -th channel of f ;
- 12: $e_i \leftarrow E(f'_i)$;
- 13: $o_i \leftarrow C(e_i)$;
- 14: $r_i \leftarrow softmax(o'_i)$;
- 15: $dis[i] \leftarrow dis[i] + abs(a - a_i)$;
- 16: **end for**
- 17: // Suppress the propagation of "noise" channels
- 18: **for** $i = 1$ to c **do**
- 19: **if** $dis[i]$ is in $maxk(dis)$ **then**
- 20: $f''[i] \leftarrow f'[i]$
- 21: **else**
- 22: $f''[i] \leftarrow 0$
- 23: **end if**
- 24: **end for**
- 25: $e'' \leftarrow E(f'')$;
- 26: $o'' \leftarrow C(e'')$;
- 27: $Gradient_{c1} \leftarrow \nabla_{\theta_g, \theta_c} \mathcal{L}_c(o, y)$
- 28: // using PA-Adaption loss
- 29: $Gradient_t \leftarrow \nabla_{\theta_g, \theta_c} \mathcal{L}_t(e'', a)$
- 30: $Gradient_{c2} \leftarrow \nabla_{\theta_g, \theta_c} \mathcal{L}_c(o'', y)$
- 31: $Gradient \leftarrow \lambda_1 Gradient_t + \lambda_2 Gradient_{c1} + \lambda_3 Gradient_{c2}$
- 32: Update $\theta_g \leftarrow \theta_g - \alpha * Gradient$
- 33: Update $\theta_e \leftarrow \theta_e - \alpha * Gradient$
- 34: Update $\theta_c \leftarrow \theta_c - \alpha * Gradient$
- 35: **end for**
- 36: **end for**

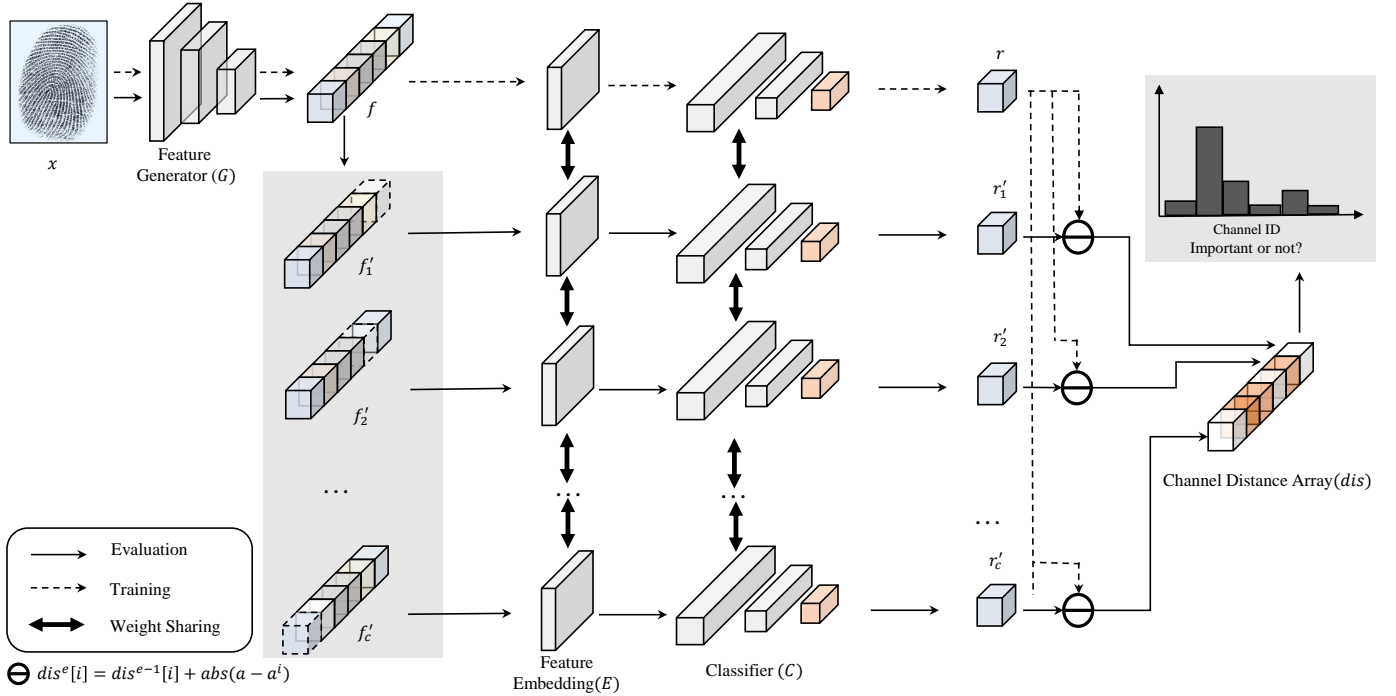


Fig. 3. Illustration of weighting the importance of each channel in the feature map f . The feature maps f'_i of the gray background is derived from suppressing each channel in the feature map f . And the importance of each channel can be obtained by calculating the distance between r and each element in r'_i (i is range from 1 to c). The output r'_i is derived after f'_i passes through the $E(\cdot)$ and $C(\cdot)$.

feature map output by $G(\cdot)$ and e denotes the feature map output by $E(\cdot)$. So we have the follow equations:

$$g = G(x) \quad (1)$$

$$e = E(g) \quad (2)$$

$$o = C(e) \quad (3)$$

where o denotes the prediction result of the network and we can get r when using the softmax function to normalize o , as formulated in Eq.(4).

$$r = \text{softmax}(o) \quad (4)$$

The system mainly consists of three steps during training, as shown in Fig.2, i.e., importance evaluation of each channel, propagation suppression of "noise" channels in the feature map, and domain alignment in channel-wise. As detailed in the Algorithm. 1, input an image x , we get a feature map f from $G(\cdot)$ by Eq.(1) in the first step. And then a channel distance array dis is generated according to the importance of each channel in the feature map f . In the second step, according to dis , we can divide channels into important channels and "noise" channels. And then we can get f'' after suppressing those "noise" channels in f in the channel suppression module by:

$$f''[i] = \begin{cases} f[i], & dis[i] \in \text{maxk}(dis) \\ 0, & dis[i] \notin \text{maxk}(dis) \end{cases} \quad (5)$$

where i denotes the i -th channel in the feature map and $\text{maxk}(\cdot)$ denotes the top k values in an array. In the channel-

wise domain alignment step, e'' which derived by Eq.(2) is put to the PA-Adaption loss for gradient updation.

B. Importance Calculation For Each Channel

The process of calculating the importance of each channel can guide the network to distinguish between important channels and "noise" channels in f . The detailed description of this process is shown in Figure 3.

Given an input image x , we first pass it into the feature generator $G(\cdot)$ to gain a feature map f . The derived feature map f has c channels and then we successively zero the value of channel i (range from 1 to c) in the feature map f but remain unchanged of other channels. So we obtain c new feature maps $\{f'_1, f'_2, \dots, f'_c\}$. Next, we feed the original feature map f and all c new feature maps $\{f'_1, f'_2, \dots, f'_c\}$ into the feature embedding layer $E(\cdot)$, the classification layer $C(\cdot)$ and the softmax layer, and thus get corresponding representation r , $\{r'_1, r'_2, \dots, r'_c\}$. Finally, we can get the channel distance array dis by calculating the distance of representation r and r'_i (i is range from 1 to c), where r is a two-tuple matrix and $r = \{a, b\}$. Since PAD is a binary classification task such as live and spoof, a and b in r denote the probability of live and spoof fingerprints respectively. The value of a and b are all range from 0 to 1, and the sum of a and b are 1. Therefore, the distance array dis can be calculated by:

$$dis^b[i] = dis^{b-1}[i] + \text{abs}(a - a_i) \quad (6)$$

where $dis^b[i]$ indicates the importance of the i -th channel in f and b denotes the batch number. Since the calculation of dis is

a cumulative process, $dis^{b-1}[i]$ denotes the calculation result of the top $(b-1)$ batch. When training starts, that is, $b=1$, and the value of $dis^{b-1}[i]$ is 0. The value $abs(a-a_i)$ describes the change of the network's output caused by suppressing the i -th channel of f . If the channel i is indeed important, the corresponding representation r'_i derived from $E(\cdot)$ and $C(\cdot)$ will change a lot compare with r . The distance $abs(a-a_i)$ between representation r and r'_i is a dynamic value. The larger the value of $abs(a-a_i)$, the suppression of the i -th channel has a more significant influence on the result, which also indicates that this channel belongs to important channels. Inversely, the small value of $abs(a-a_i)$ means that the network output is not sensitive to suppressing the i -th channel, which illustrates that the i -th channel is a "noise" channel. Since evaluating the importance of each channel is a dynamic accumulation process, the importance of each channel in the e -th batch is jointly determined by the current batch and the previous $(b-1)$ batch together.

We calculate the importance of each channel in f to get c values $dis = \{dis[1], dis[2], \dots, dis[k], \dots, dis[c]\}$ and we sort dis by their value. More formally, $maxk(\cdot)$ function means the top k values in an array and we select the top k channels as important channels. Correspondingly, the rest $(c-k)$ channels belong to "noise" channels. In addition, dis is a dynamically accumulated channel distance array, we accumulate the distance between r and r'_i (i is range from 0 to c) in every batch.

C. Channels Suppression

Since all the channels in f are divided into important channels and "noise" channels according to dis , the process of channels suppression is to suppress the propagation of "noise" channels and keep important channels unchanged. After suppressing those "noise" channels in f we can get f'' .

The channel distance array dis indicates the importance of each channel in the feature map f . dis is an array containing c elements, each element in dis represents the importance of the corresponding channel in f . Using $maxk()$ to select the top- k value in dis and the index of the k values is the number id of important channels in f . While the remaining belong to "noise" channels. There exist abundant discriminative features in important channels and "noise" features in "noise" channels. To eliminate the reflection of "noise" features, we set 0 to those "noise" channels in f , while remain unchanged of other important channels, as list in Eq(5). Since the corresponding gradient will disappear after setting 0 to those "noise" channels, which achieve the goal of denoising. We get f'' after denoising the feature map f and the denoised feature map f'' will replace f to propagate in the network. When f'' passing through $E(\cdot)$ and $C(\cdot)$, we can get e'' and o'' by Eq.(2) and Eq.(3).

D. Design of PA-Adaption Loss

Due to the diversity of attack materials and sensors, the distribution discrepancies are much larger among spoof than live fingerprints. Therefore, seeking a generalized feature

domain for the spoof fingerprints is difficult and may also affect the classification accuracy for the target domain. In consideration of this, we proposed to align the feature domain of fingerprints by pulling all the live fingerprints close while pushing the spoof ones of different materials or sensors apart.

As shown in Fig.4, the feature domains of live fingerprints and spoof fingerprints of different attack materials or sensors are randomly distributed. Spoof fingerprints of different materials of sensors belong to different classes here. To aggregate the feature domains of different classes of fingerprints respectively, PA-Adaption loss is conducted on the live and spoof fingerprints to achieve the following optimization goals: Firstly, we separate the spoof fingerprints of different feature domains apart; Secondly, we pull apart the spoof fingerprints away from the live fingerprints. The constrain of PA-Adaption loss is given by:

$$\mathcal{L}_{padp} = max(\|E(f^a) - E(f^p)\|_2^2 - \|E(f^a) - E(f^n)\|_2^2 + \alpha, 0) \quad (7)$$

where the anchor f^a and the positive example f^p are all feature maps with the same label, while f^n is the feature map of a negative sample, which has a different label with f^a . The α is a margin that is enforced between positive and the negative pairs. $E(\cdot)$ denotes the feature embedding layer, and f denotes a feature map generator by the feature generator $G(\cdot)$. So, equation(7) can also be written as:

$$\mathcal{L}_{padp} = max(\|e^a - e^p\|_2^2 - \|e^a - e^n\|_2^2 + \alpha, 0) \quad (8)$$

where $\|e^a - e^p\|_2^2$ denotes the distance between anchor and positive sample, and $\|e^a - e^n\|_2^2$ denotes the distance between anchor and negative sample. We minimize this loss to push $\|e^a - e^p\|_2^2$ to 0 and $\|e^a - e^n\|_2^2$ to be greater than $\|e^a - e^p\|_2^2 + \alpha$. As soon as $\|e^a - e^p\|_2^2 + \alpha < \|e^a - e^n\|_2^2$, the loss becomes zero. After PA-Adaption loss, the extracted features of spoof fingerprints are more dispersed than before in the feature domain but the feature domain of live fingerprints is getting aggregated, which achieves good performance for unknown attack materials or sensors.

Furthermore, in order to pull all the live fingerprints close but push the spoof ones of different materials or sensors apart, we use $\mathcal{L}_{padp}(e'', a)$ to calculate their PA-Adaption loss for the gradient update. And a is a more fine-grained label compared with y . The fine-grained label a not only contains the live or false label of the input sample x but also contains the types of attack sensor or material if x is a spoof sample. e'' is a denoised feature map, which is calculated by Eq(1), Eq (2) and Eq (5). Using the denoised feature map for PA-Adaption loss can force the network less interfered by "noise" channels, which promotes the network to learn a better feature domain for unknown attack materials or sensors.

Integrating all things mentioned above together, the objective of the proposed channel-wise feature denoising method for fingerprint PAD is:

$$\mathcal{L}_{cfd} = \lambda_1 \mathcal{L}_c(o, y) + \lambda_2 \mathcal{L}_{padp}(e'', a) + \lambda_3 \mathcal{L}_c(o'', y) \quad (9)$$

where λ_1 , λ_2 and λ_3 are the balanced parameters and \mathcal{L}_c is the cross-entropy loss.

TABLE I
SPECIFICATION FOR BACKBONE: MOBILENET V2 ARCHITECTURE [48]

Input	Operator	Expansion factor	Output-Channel	Repeated times	Stride
$224 \times 224 \times 3$	conv2d	-	32	1	2
$112 \times 112 \times 32$	bottleneck	1	16	1	1
$112 \times 112 \times 16$	bottleneck	6	24	2	2
$56 \times 56 \times 24$	bottleneck	6	32	3	2
$28 \times 28 \times 32$	bottleneck	6	64	4	2
$14 \times 14 \times 64$	bottleneck	6	96	3	1
$14 \times 14 \times 96^*$	bottleneck	6	160	3	2
$7 \times 7 \times 160$	bottleneck	6	320	1	1
$7 \times 7 \times 320$	conv2d 1×1	-	1280	1	1
$7 \times 7 \times 1280$	avgpool	-	-	1	-
$1 \times 1 \times 1280$	conv2d 1×1	-	2	-	-

* The derive feature map z_t .

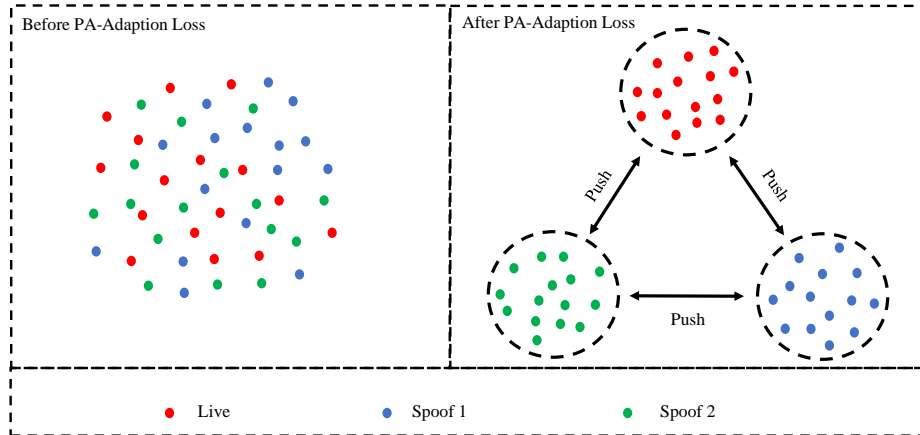


Fig. 4. Description of the PA-Adaption loss. The points in different colors represent the feature distribution of live or fake fingerprints of different attack materials or sensors. Left: Different types of fingerprints are distributed in the feature domain randomly and their distribution is irregular before PA-Adaption loss. Right: After PA-Adaption loss, the domains of different spoof fingerprints are separated while the domains of live fingerprints are aggregated. Meanwhile, the live fingerprints are also pulled apart away from all the spoof fingerprints.

III. EXPERIMENTS AND RESULTS

To evaluate the performance of the proposed method, several experiments were carried on LivDet 2017 [14] in this section, which is one of the most commonly used public datasets for fingerprint PAD. We first introduce the dataset and implementation details in subsection A. And then we show the evaluation metrics and other methods compared with us in subsection B. Subsequently, we prove the effectiveness of the proposed CFD-PAD method in subsection C. Finally, subsection D shows the comparison between our method and other current methods on LivDet 2017.

A. Dataset and Implementation Details

Table II presents a summary of the LivDet 2017 dataset. LivDet 2017 dataset is one of the most recent publicly available LivDet datasets, containing over 17,500 fingerprint images captured from three different scanners, namely Green Bit, Orcanthus, and Digital Persona. Unlike other LivDet datasets, the spoof materials in the training set and testing set are completely different. In the training set, the spoof materials are Wood Glud, Ecoflex and, Body Double. In the testing set, the spoof materials are Latex, Gelatine and, Liquid Ecoflex. As shown in Table II, there are about 2200 images for training

and 3740 images for testing for each sensor. In the training set and testing set, the number of each attack material is about 400 and 680, respectively. LivDet 2017 is a suitable cross-dataset to evaluate the generalization performance of PAD methods.

To promote network to learn non-local features, we use the cut-out module to perform the data pre-processing. Inspired by [49], we randomly select a pixel coordinate within the image as a center point and then place the zero-mask around that location in the training stage. The size of the zero-mask is set to 96×96 and the number of zero-masks is 10. Besides, data augmentation techniques, including horizontal flipping, vertical flipping, and random rotation are adopted to ensure that the trained model is robust to the possible variations in fingerprint images.

MobileNet v2 [48] pretrained on ImageNet [50] is used as backbone for the proposed CFD-PAD method. For feature generator $G(\cdot)$, feature embedding $E(\cdot)$, and classifier $C(\cdot)$, they are all substructures of MobileNet v2. As shown in Table I, the feature embedding $E(\cdot)$ contains a bottleneck layer and a conv2d 1×1 layer. Compared with the other popular deep networks, MobileNet v2 is particularly suitable for mobile applications. It allows very memory-efficient inference and relies on utilizing standard operations present in all neural frameworks, which is proved to be useful for fingerprint PAD

TABLE II
SUMMARY OF THE LIVDET 2017 DATASETS [14]

Sensor	Images				Model	Type	Resolution(dpi)	Image Size	Spoof Material for Training	Spoof Material for Testing
	Train(Live/Spoof)		Test(Live/Spoof)							
GreenBit	1000	1200	1700	2040	DactyScan84c	Optical	500	500 × 500	Wood Glue,	Gelatine,
DigitalPersona	999	1199	1700	2028	U.are.U 5160	Optical	500	252 × 324	Exoflex,	Liquid Ecoflex,
Orcanthus	1000	1200	1700	2018	Certis2 Imag	Thermal swipe	500	300 × n	Body Double	Latex

in [51]. On the basis of network architecture search (NAS), MobileNet v2 uses a combination of depth-wise separable convolutions [52–54], linear bottlenecks, inverted residuals, and information flow interpretation as building blocks. The architecture of linear bottleneck captures the low-dimensional manifold of interest by inserting linear bottleneck layers into the convolutional blocks and uses linear layers to prevent non-linearities from destroying too much information. In the inverted residual, denotes as the bottleneck, Sandler [48] et al. use shortcuts directly between the bottlenecks because the bottlenecks contain all the necessary information, while an expansion layer acts merely as an implementation detail that accompanies a non-linear transformation of the tensor. As the specification listed in TABLE I, the backbone used in this paper is called MobileNet v2, which consists of 17 bottlenecks, 2 convolutional layers and, 1 average pooling layer. Since the sizes of fingerprint images derived from the various sensors are different, the average pooling layer (i.e. avgpool in TABLE I) is used to handle arbitrary sizes of input fingerprints images. Besides, the last layer of the original architecture, a convolutional layer with 1000-unit output, is replaced by the convolutional layer with a 2-unit output of fingerprint PAD, i.e. live fingerprint and spoof fingerprint.

Our implementation is based on the public platform Pytorch [55]. We use the Adam optimizer for training and the learning rate of the Adam is set to 0.0001. The feature map f that derived after the feature generator is shown in Table I marked by *, the shape of f is $(7 \times 7 \times 160)$ if the input x is $(224 \times 224 \times 3)$. The feature map f has a total of 160 channels, and the number of important channels k is set to 30. Our workstation’s CPU is 2.8GHz, RAM is 32GB and GPU is NVIDIA TITAN RTX.

B. Evaluation Metrics and Comparison Method

To evaluate the performance of the methods, two popular metrics like Average Classification Error (ACE) and True Detection Rate (TDR) @ False Detection Rate (FDR) = 1% are used. Among them, ACE reflects the classification performance of the method. The smaller the value of ACE, the better the performance of the evaluation method. While TDR@FDR=1% represents the percentage of PAs able to breach the biometric system security when the reject rate of legitimate users $\leq 1\%$. The larger the value of TDR@FDR=1%, the better performance the evaluated method achieves. To further demonstrate the performance of our method, we compare it with single model based methods and multiple model based methods. The single model based methods include the winner in LivDet 2017 [14], and FSB [1]. Similar, we compared our

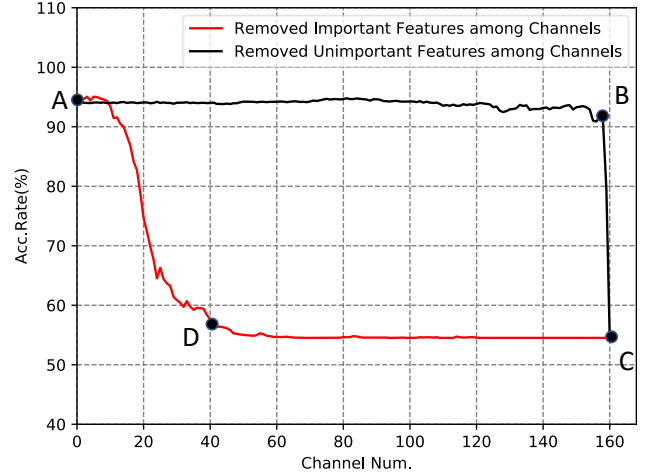


Fig. 5. Accuracy after removing different channels. The black line in the figure shows the accuracy after removing “noise” features among channels. The red line in the figure shows the accuracy after removing important features among channels.

method with multiple model based methods, i.e., FSB + UMG Wrapper [35] and RTK-PAD [32].

C. Effectiveness Validation of the Proposed CFD-PAD Method

To verify the effectiveness of our method, we trained a CNN for PAD and derived a feature map at the middle layer of the trained CNN. The derived feature map has a total of 160 channels, and a large number of features extracted from discriminative regions and noise regions are preserved in the feature map. As shown in Fig. 5, when some important features or “noise” feature among channels are removed respectively, the accuracy of PAD has become different. The red line in the figure shows the accuracy after removing important features among channels and the black line shows the accuracy after removing “noise” features among channels. When about 20 important features among channels are removed, the accuracy of PAD has dropped from over 90 to less than 80, which decline significantly. After removing nearly 40 important channels, the network can hardly be classified correctly. In contrast, the changes in accuracy for removing “noise” features among channels are quite different. As shown in the black line, the accuracy of removing the first 150 “noise” features among channels does not change significantly. The classification accuracy starts to drop until more than 150 “noise” features among channels are removed. The above experimental results illustrate that there exist “noise” and important features in the

TABLE III
PERFORMANCES OF CFD-PAD WITH OR WITHOUT EACH PROPOSED MODULE IN TERMS OF ACE AND TDR@FDR=1.0%

Baseline	PA-Adaption Loss	Channel-wise Feature Denoising	Channel-wise Feature Regularization	LivDet 2017							
				GreenBit		Orcanthus		DigitalPersona		Mean	
				ACE(%)	TDR(%)	ACE(%)	TDR(%)	ACE(%)	TDR(%)	ACE(%)	TDR(%)
✓	×	×	×	3.54	81.67	2.94	71.46	4.83	68.64	3.77 ± 0.97	73.92 ± 6.86
✓	✓	×	×	2.93	88.08	2.67	82.61	4.72	76.53	3.44 ± 1.12	82.41 ± 5.78
✓	×	✓	×	3.36	86.72	2.27	84.59	4.61	71.80	3.41 ± 1.17	81.04 ± 8.07
✓	✓	×	✓	3.00	90.81	2.60	86.67	4.79	76.33	3.46 ± 1.16	84.60 ± 7.46
✓	✓	✓	×	2.59	93.43	1.68	97.32	3.33	90.73	2.53 ± 0.82	93.83 ± 3.31

TABLE IV
PERFORMANCE COMPARISON BETWEEN THE PROPOSED METHOD AND STATE-OF-THE-ART RESULTS REPORTED ON LIVDET2017 DATASET FOR CROSS MATERIAL EXPERIMENTS IN TERMS OF ACE AND TDR@FDR=1.0%

LivDet 2017	Single Model				Multiple Model				
	LivDet 2017 Winner [14]	FSB [1]		CFD-PAD (Ours)		FSB + UMG [35]		RTK-PAD [32]	
	ACE(%)	ACE(%)	TDR(%)	ACE(%)	TDR(%)	ACE(%)	TDR(%)	ACE(%)	TDR(%)
GreenBit	3.56	3.32	91.07	2.59	93.43	2.58	92.29	1.92	96.82
Digital Persona	6.29	4.88	62.29	3.33	90.73	4.80	75.47	3.25	80.57
Orcanthus	4.41	5.49	66.59	1.68	97.32	4.99	74.45	1.67	96.18
Mean ± s.d.	4.75 ± 1.40	4.56 ± 1.12	73.32 ± 15.52	2.53 ± 0.82	93.83 ± 3.31	4.12 ± 1.34	80.74 ± 10.02	2.28 ± 0.69	91.19 ± 7.51

TABLE V
PERFORMANCE COMPARISON BETWEEN THE PROPOSED METHOD AND STATE-OF-THE-ART RESULTS REPORTED ON LIVDET2017 DATASET FOR CROSS-SENSOR EXPERIMENTS IN TERMS OF ACE AND TDR@FDR=1.0%

LivDet 2017		Single Model				Multiple Model	
Training Sensor	Testing Sensor	FSB [1]		CFD-PAD(Ours)		RPK-PAD [32]	
		ACE(%)	TDR(%)	ACE(%)	TDR(%)	ACE(%)	TDR(%)
GreenBit	Orcanthus	50.57	0.00	22.34	21.56	30.49	20.61
GreenBit	DigitalPersona	10.63	57.48	7.03	75.05	7.41	70.41
Orcanthus	GreenBit	30.07	8.02	30.92	2.87	28.81	15.00
Orcanthus	DigitalPersona	42.01	4.97	27.44	4.78	29.19	13.26
DigitalPersona	GreenBit	10.46	57.06	6.23	66.57	6.74	70.25
DigitalPersona	Orcanthus	50.68	0.00	24.83	23.09	28.55	18.68
Mean ± s.d.		32.40 ± 18.53	21.26 ± 28.06	19.80 ± 10.59	32.32 ± 31.07	21.87 ± 10.48	34.70 ± 25.30

feature map simultaneously, which is similar to the "noise" and discriminative regions. The channels in the feature map that contains abundant features can be deemed as important channels, while the remaining are "noise" channels. The discriminative regions correspond to those important channels between points A and B on the red line in Fig 5. The important channels are discriminative, they contain abundant features of the fingerprints and have a positive effect on the prediction results of the module. On the contrary, the "noise" channels in Fig 5, which corresponds to point A to D on the black line, are similar to the "noise" regions. "Noise" channels contain a lot of invalid and redundant "noise" features which will greatly interfere with the prediction results of the network. Successfully removing the influence of "noise" features may perfectly improve the performance of the model on PAD.

We also perform the ablation study to evaluate the cross-material performance gained by each module for different network architectures, i.e., PA-Adaption loss and channel-wise feature denoising on the LivDet 2017. Table III and Fig. 6 present the generalization performance of the proposed method when all the training and testing images are captured using the same sensor but the spoof materials in the training and testing set are completely different. Table III is the ablation study result of our method, it can be seen that the PA-Adaption loss module and channel-wise feature denoising module can improve the performance effectively. To visualize the ablation

study, we plot the ROC curves for GreenBit, DigitalPersona, and Orcathus respectively. As shown in Fig. 6, the "PA Loss + CFD(Ours)" line achieved the best results in all three cases, which indicates the effectiveness of our proposed method.

To quantify the contribution of PA-Adaption loss, we compare the baseline with the results by adding PA-Adaption loss to the baseline. Table III shows the result after adding the PA-Adaption loss to baseline, ACE decrease from 3.77% to 3.44%, and TDR@FDR=1.0% improve from 73.92% to 82.41%. On the contrary, after removing PA-Adaption loss on "Channel-wise Feature Denoising + PA-Adaption Loss", ACE increase from 2.53% to 3.41%, and TDR@FDR=1.0% decline from 91.68% to 81.04%. The results indicate that PA-Adaption loss has successfully modified the feature distribution of live and spoof fingerprints by pulling all the live fingerprints aggregated while pushing the spoof ones of different materials apart. This proves that PA-Adaption loss can improve the performance of the baseline effectively.

Since the channel-wise feature denoising module is an important part of the method, we also test the contribution of the channel-wise feature denoising module and the result is listed in Table III. Compared with baseline, the method using channel-wise feature denoising has better performance, ACE is decreased from 3.77% to 3.41% and TDR@FDR=1.0% is improved from 73.92% to 81.04%. However, when the channel-wise feature denoising module is removed from the

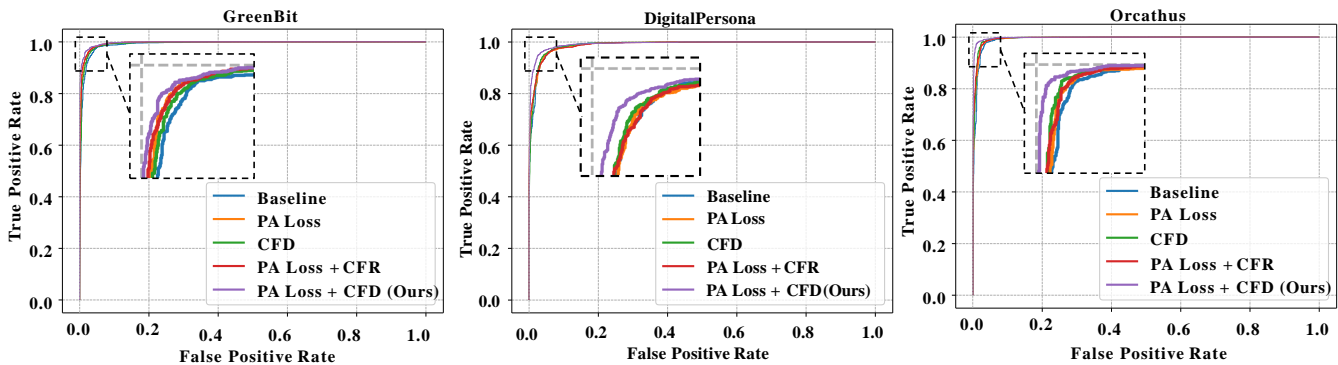


Fig. 6. ROC curves for the ablation study on fingerprint PAD. PA Loss denotes the PA-Adaption loss, CFD denotes the channel-wise feature denoising and CFR denotes the channel-wise feature regularization.

final experiment, it is observed that the ACE is increased from 2.53% to 3.44%, and TDR@FDR=1.0% is declined from 93.83% to 82.41%. This result demonstrates that the channel-wise feature denoising module can remove redundant "noise" features in the fingerprint, which shows the effectiveness of the channel-wise feature denoising.

To further verify the effectiveness of the channel-wise feature denoising module, we compared it with the channel-wise feature regularization module. Channel-wise feature denoising and channel-wise feature regularization are similar in the process of evaluating the importance of each channel. dis is calculated which can reflect the importance of each channel in the module of channel-wise feature regularization and channel-wise feature denoising. But the difference is that channel-wise feature regularization chooses the down k channels in dis as important channels and the rest are "noise" channels, while channel-wise feature denoising chooses the top k channels in dis as important channels and the rest are "noise" channels. The result in Table III shows that channel-wise feature regularization achieves the ACE of 3.46% and TDR@FDR=1.0% of 84.60%, which did not get a good performance compared with channel-wise feature denoising. This result demonstrates that compared with channel-wise feature regularization, channel-wise feature denoising is more useful and can improve the performance effectively.

In order to investigate the advance of the proposed method, we adopt the Grad-CAM to provide the class activation map(CAM) visualizations of our method and baseline, which has the same architecture as our method but without denoising module. As shown in Fig. 7, the first two row shows the live sample, and the last two row presents the spoof sample. The first column is the original image, the second column is the visualization results after using the denoising method, and the last column is the visualization result without using the denoising method (undenoising method). We can see that CFD-PAD always focuses on the adequate region of interest(ROI) for both live and spoof fingerprints to seek discriminative cues instead of domain-specific backgrounds, which is more likely to generalize well to unseen domains. However, when compared with the pre-trained model from the denoising method, the undenoising method localize some

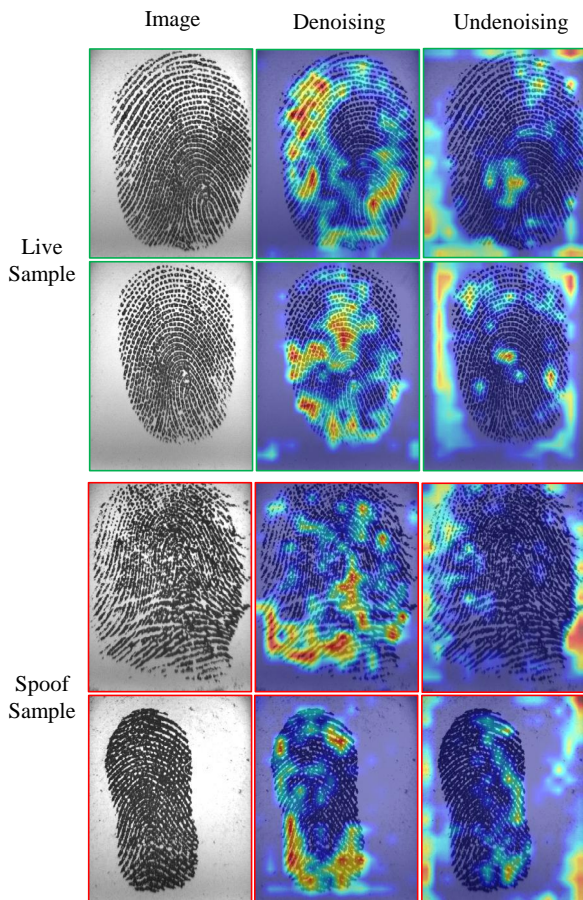


Fig. 7. Grad-CAM visualizations on LivDet2017 under Digital Persona. The first two row shows the live sample and the last two row presents the spoof sample. The first column is the original image, the second column is the visualization results after using the denoising method, and the last column is the visualization result without using the undenoising method.

background region, which indicates the effectiveness of the proposed denoising method.

D. Comparison With Existing Methods

To demonstrate the performance of our CFD-PAD method, we compare it with other single and multiple model based PAD methods, i.e., the winner in LivDet 2017 [14], a minutiae-

centered patches based method [1], a style-transfer based method [35], the state-of-the-art PAD method [32] et al. Table IV and Table V present the performance of some fingerprint PAD methods on LivDet 2017. The performance of our proposed CFD-PAD method achieves 2.53% ACE and 93.83% TDR@FDR=1% in the cross-material setting and achieves 19.80% ACE and 32.32% TDR@FDR=1% in the cross-material setting.

In this paper, two different experimental settings are considered, including cross-material and cross-sensor. In the case of cross-material, the spoof materials used in the training set and testing set are different, as shown in Table II. The spoof materials in the training set are Wood Glue, Ecoflex, Body Double but Gelatine, Latex, Liquid Ecoflex in the testing set. Therefore, the data partition of LivDet 2017 can be directly used as the cross-material setting. In the case of cross-sensor, the fingerprint images in the training set and testing set use different sensors.

1) In The Case of Cross-Material:

Table IV presents the generalization performance of the proposed method on the LivDet2017 dataset in the case of cross-material. A significant reduction in the mean of ACE is achieved by the proposed method. In the case of cross-material, compared with the best single model based method Fingerprint Spoof Buster (FSB) [1], the mean ACE is reduced from 4.56% to 2.53% and the mean TDR@FDR=1% is improved from 73.32% to 93.83% by our method. A 44.52% reduction in the mean of ACE and a 27.97% rise in the mean of TDR@FDR=1% are achieved by our method compared with FSB. Compared with the best multiple model based model RTK-PAD [32], the mean of TDR@FDR=1% is improved from 91.19% to 93.83% and our method has achieved the state-of-the-art method performance in TDR@FDR=1%.

In the case of Orcanthus, the proposed method outperforms the combination of Fingerprint Spoof Buster and UMG wrapper by a wide margin. When using Orcanthus as the training and testing sensor, our proposed method can achieve 1.68% ACE, which improves obviously compared with the previous method [1, 14, 35]. When Orcanthus is used as the sensor, our method decreases 2.73% in the ACE compared to LivDet 2017 Winner [14] which is the best single model based method in the case of Orcanthus before. Given Digital Persona as the sensor, the ACE of our method is 3.33%, which is also better than the best single model based method before [35]. Compared with the single model based methods, we can see that the proposed method outperforms all the single model based methods by a wide margin in the evaluation metrics of both ACE and TDR@FDR=1%. Compared with multiple model based methods, we can still get a good performance at the same time. Even if we use a single model, we can fully beyond the combination of Fingerprint Spoof Buster and the style-transfer based wrapper (FSB + UMG) [35] in both ACE and TDR@FDR=1%. In the evaluation metric of TDR@FDR=1%, our method has improved from 91.19% to 93.83% compared with the state-of-the-art method RTK-PAD [32]. Experimental results indicate that the proposed CFD-PAD method has better performance and generalization ability

in PAD, and has achieved the state-of-the-art performance on LivDet 2017 in TDR@FDR=1%.

2) In The Case of Cross-Sensor:

We compare the performance of the proposed method with Fingerprint Spoof Buster [1] and RTK-PAD method [32] under cross-sensor setting to further verify the robustness of the proposed method. In the case of cross-sensor, the sensors used in the training set and testing set are completely different. Since there are three types of sensors, we conducted 6 sets of experiments in order to cover all of their combinations. As the results show in Table V, the proposed method achieves the best performance in the mean of ACE. More specifically, compared with the best single model based method [1], we achieve better performance in both ACE and TDR@FDR. While compared with the current best multiple model based method, i.e. RTK-PAD [32], we still get a better performance in terms of ACE (19.80% vs. 21.87%) .

It should be noted that FSB+UMG [35] is a style transfer based method, which also tests in cross-sensor setting. This method uses the UMG framework to augment CNN-based spoof detector(FSB), which significantly improves the performance of FSB against novel materials while retaining its performance on known materials [1, 35]. However, their method uses the data in the target sensor to synthesize extra data [35] while we do not use the data in the target sensor, it is unfair to compare our method with FSB + UMG [35]. FSB + UMG wrapper can achieve 19.37% in ACE and 43.23% in TDR@FDR=1% in the case of cross-sensor setting. But our method reaches to an accuracy close to FSB + UMG wrapper (e.g. 19.80% vs. 19.37% [35] in terms of ACE) but without using any image from target sensor. Thus we conclude that even without using the data derived from target sensors, our method can also improve the cross-sensor performance effectively.

TABLE VI
COMPUTATIONAL COMPLEXITY IN TERMS OF PARAMS AND TIME COST.

	Input Size	FLOPs (GMACs)	Time Cost (ms)
FSB [1]	~48×224×224×3	~27.84	268.2
RTK-PAD [32]	1×224×224×3	0.69	237.3
CFD-PAD (Ours)	1×224×224×3	0.31	59.9

E. Computational Complexity Analysis

To investigate the computational complexity of the proposed method, we calculate the FLOPs (floating point operations) and time cost as the evaluation metrics. As list in Table VI, both Time Cost and FLOPs of the proposed method are less than FSB [1] and the state-of-the-art method, RTK-PAD [32]. FSB [1] is a single model based method, which needs to calculate the spoof score of 48 minutiae-centered patches and fusion their scores, no such operations are needed by our method. Hence, a 208.3 ms reduction in terms of time cost can be saved by our method. RTK-PAD [32] is a multiple model based method, which uses a global PAD module, a local PAD module, and a rethinking module, but our method only uses a single model. Hence, our method spends less time

than RTK-PAD. When input size is $1 \times 224 \times 224 \times 3$, our method takes 59.9ms to distinguish spoof from live fingerprints, which is faster than RTK-PAD markedly. Our method is based on a single lightweight model, which is time-saving and suitable for deployment conditions. Compared with RTK-PAD, a 74.76% reduction in time-consuming is achieved by our method. Hence, whether compared with other single model or multiple model based method, far less time is required by our method.

IV. CONCLUSION

Improving the robustness and generalization ability of PAD methods is critical to ensure the security of a fingerprint recognition system. This paper thus proposes a channel-wise feature denoising method and a PA-Adaption loss. The method contains three key steps during training, including each channel's importance evaluation, "noise" channels' suppression and, channel-wise domain alignment. In the stage of channels evaluation, the importance of each channel is quantified according to the change of the results after the channel is suppressed. And then all the channels in the feature map can be divided into important channels and "noise" channels. The influence of "noise" features among channels will be greatly reduced due to the suppression of the propagation of "noise" channels. Finally, a PA-Adaption loss is designed to constrain the feature distribution. The effectiveness of the proposed method was proved by experiments on LivDet 2017, which is one of the most recent publicly available LivDet datasets. Our experimental results have shown that compared with baseline, PA-Adaption loss has reduced the evaluation metric of ACE from 3.77% to 3.44% and increased TDR@FDR=1% from 73.92% to 82.41%. Similarly, the channel-wise feature denoising module has reduced ACE from 3.77% to 3.41% and increased TDR@FDR=1% from 73.92% to 81.04%. The combination of channel-wise feature denoising and PA-Adaption loss can achieve 2.53% ACE and 93.83% TDR@FDR=1%, which get a better result compared with adding PA-Adaption loss module and channel-wise feature denoising module respectively. The effectiveness of the propose method is further proved by comparing with the state-of-the-art PAD methods under cross material and cross sensor settings.

V. ACKNOWLEDGMENT

This work is supported in part by National Natural Science Foundation of China under Grant 62076163 and Grant 91959108; In part by the Shenzhen Fundamental Research Fund under Grant JCYJ20190808163401646 and Grant JCYJ20180305125822769; And in part by the Tencent Rhinoceros Birds-Scientific Research Foundation for Young Teachers of Shenzhen University.

REFERENCES

- [1] T. Chugh, K. Cao, and A. K. Jain, "Fingerprint spoof buster: Use of minutiae-centered patches," *IEEE Transactions on Information Forensics and Security*, vol. 13, no. 9, pp. 2190–2202, 2018.
- [2] F. Liu, H. Liu, W. Zhang, G. Liu, and L. Shen, "One-class fingerprint presentation attack detection using auto-encoder network," *IEEE Transactions on Image Processing*, vol. 30, pp. 2394–2407, 2021.
- [3] D. Maltoni, D. Maio, A. K. Jain, and S. Prabhakar, *Handbook of fingerprint recognition*. Springer Science & Business Media, 2009.
- [4] S. Marcel, M. S. Nixon, and S. Z. Li, *Handbook of biometric anti-spoofing*. Springer, 2014, vol. 1.
- [5] F. Liu, G. Liu, and X. Wang, "High-accurate and robust fingerprint anti-spoofing system using optical coherence tomography," *Expert Systems with Applications*, vol. 130, pp. 31–44, 2019.
- [6] T. Chugh, K. Cao, and A. K. Jain, "Fingerprint spoof detection using minutiae-based local patches," in *2017 IEEE International Joint Conference on Biometrics (IJCB)*. IEEE, 2017, pp. 581–589.
- [7] S. S. Arora, K. Cao, A. K. Jain, and N. G. Paulter, "Design and fabrication of 3d fingerprint targets," *IEEE Transactions on Information Forensics and Security*, vol. 11, no. 10, pp. 2284–2297, 2016.
- [8] S. S. Arora, A. K. Jain, and N. G. Paulter, "Gold fingers: 3d targets for evaluating capacitive readers," *IEEE transactions on information forensics and security*, vol. 12, no. 9, pp. 2067–2077, 2017.
- [9] J. J. Engelsma, S. S. Arora, A. K. Jain, and N. G. Paulter, "Universal 3d wearable fingerprint targets: advancing fingerprint reader evaluations," *IEEE Transactions on Information Forensics and Security*, vol. 13, no. 6, pp. 1564–1578, 2018.
- [10] I. Goicoechea-Telleria, B. Fernandez-Saavedra, and R. Sanchez-Reillo, "An evaluation of presentation attack detection of fingerprint biometric systems applying iso/iec 30107-3," in *International Biometric Performance Testing Conference*, 2016.
- [11] T. Chugh and A. K. Jain, "Oct fingerprints: Resilience to presentation attacks," *arXiv preprint arXiv:1908.00102*, 2019.
- [12] L. Ghiani, D. A. Yambay, V. Mura, G. L. Marcialis, F. Roli, and S. A. Schuckers, "Review of the fingerprint liveness detection (livdet) competition series: 2009 to 2015," *Image and Vision Computing*, vol. 58, pp. 110–128, 2017.
- [13] V. Mura, L. Ghiani, G. L. Marcialis, F. Roli, D. A. Yambay, and S. A. Schuckers, "Livdet 2015 fingerprint liveness detection competition 2015," in *2015 IEEE 7th International Conference on Biometrics Theory, Applications and Systems (BTAS)*, 2015, pp. 1–6.
- [14] V. Mura, G. Orrù, R. Casula, A. Sibiriu, G. Loi, P. Tuveri, L. Ghiani, and G. L. Marcialis, "Livdet 2017 fingerprint liveness detection competition 2017," in *2018 International Conference on Biometrics (ICB)*. IEEE, 2018, pp. 297–302.
- [15] E. Marasco and A. Ross, "A survey on antispoofing schemes for fingerprint recognition systems," *ACM Computing Surveys (CSUR)*, vol. 47, no. 2, pp. 1–36, 2014.
- [16] C. D. Robison and M. S. Andrews, "System and method of fingerprint anti-spoofing protection using multi-spectral optical sensor array," Mar. 26 2019, uS Patent 10,242,245.
- [17] R. Tolosana, M. Gomez-Barrero, J. Kolberg, A. Morales, C. Busch, and J. Ortega-Garcia, "Towards fingerprint presentation attack detection based on convolutional neural networks and short wave infrared imaging," in *2018 International Conference of the Biometrics Special Interest Group (BIOSIG)*. IEEE, 2018, pp. 1–5.
- [18] R. Tolosana, M. Gomez-Barrero, C. Busch, and J. Ortega-Garcia, "Biometric presentation attack detection: Beyond the visible spectrum," *IEEE Transactions on Information Forensics and Security*, vol. 15, pp. 1261–1275, 2019.
- [19] Y. Moolla, L. Darlow, A. Sharma, A. Singh, and J. Van Der Merwe, "Optical coherence tomography for fingerprint presentation attack detection," in *Handbook of Biometric Anti-Spoofing*. Springer, 2019, pp. 49–70.
- [20] D. Baldisserra, A. Franco, D. Maio, and D. Maltoni, "Fake fin-

- gerprint detection by odor analysis,” in *International Conference on Biometrics*. Springer, 2006, pp. 265–272.
- [21] K. A. Nixon, R. K. Rowe, J. Allen, S. Corcoran, L. Fang, D. Gabel, D. Gonzales, R. Harbour, S. Love, R. McCaskill *et al.*, “Novel spectroscopy-based technology for biometric and liveness verification,” in *Biometric Technology for Human Identification*, vol. 5404. International Society for Optics and Photonics, 2004, pp. 287–295.
- [22] P. V. Reddy, A. Kumar, S. Rahman, and T. S. Mundra, “A new antispoofing approach for biometric devices,” *IEEE transactions on biomedical circuits and systems*, vol. 2, no. 4, pp. 328–337, 2008.
- [23] M. Agassy, B. Castro, A. Lerner, G. Rotem, L. Galili, and N. Altman, “Liveness and spoof detection for ultrasonic fingerprint sensors,” Apr. 16 2019, uS Patent 10,262,188.
- [24] F. Liu, C. Shen, H. Liu, G. Liu, Y. Liu, Z. Guo, and L. Wang, “A flexible touch-based fingerprint acquisition device and a benchmark database using optical coherence tomography,” *IEEE Transactions on Instrumentation and Measurement*, vol. 69, no. 9, pp. 6518–6529, 2020.
- [25] J. J. Engelsma, K. Cao, and A. K. Jain, “Raspireader: Open source fingerprint reader,” *IEEE transactions on pattern analysis and machine intelligence*, vol. 41, no. 10, pp. 2511–2524, 2018.
- [26] S. Schuckers and P. Johnson, “Fingerprint pore analysis for liveness detection,” Nov. 14 2017, uS Patent 9,818,020.
- [27] J. Jia, L. Cai, K. Zhang, and D. Chen, “A new approach to fake finger detection based on skin elasticity analysis,” in *International Conference on Biometrics*. Springer, 2007, pp. 309–318.
- [28] A. Antonelli, R. Cappelli, D. Maio, and D. Maltoni, “Fake finger detection by skin distortion analysis,” *IEEE Transactions on Information Forensics and Security*, vol. 1, no. 3, pp. 360–373, 2006.
- [29] Z. Xia, C. Yuan, R. Lv, X. Sun, N. N. Xiong, and Y.-Q. Shi, “A novel weber local binary descriptor for fingerprint liveness detection,” *IEEE Transactions on Systems, Man, and Cybernetics: Systems*, vol. 50, no. 4, pp. 1526–1536, 2018.
- [30] H.-s. Lee, H.-j. Maeng, and Y.-s. Bae, “Fake finger detection using the fractional fourier transfchugh2019fingerprintorm,” in *European Workshop on Biometrics and Identity Management*. Springer, 2009, pp. 318–324.
- [31] S. B. Nikam and S. Agarwal, “Fingerprint liveness detection using curvelet energy and co-occurrence signatures,” in *2008 fifth international conference on computer graphics, imaging and visualisation*. IEEE, 2008, pp. 217–222.
- [32] H. Liu, W. Zhang, F. Liu, H. Wu, and L. Shen, “Fingerprint presentation attack detector using global-local model,” *IEEE Transactions on Cybernetics*, 2021.
- [33] R. F. Nogueira, R. de Alencar Lotufo, and R. C. Machado, “Fingerprint liveness detection using convolutional neural networks,” *IEEE transactions on information forensics and security*, vol. 11, no. 6, pp. 1206–1213, 2016.
- [34] D. Menotti, G. Chiachia, A. Pinto, W. R. Schwartz, H. Pedrini, A. X. Falcao, and A. Rocha, “Deep representations for iris, face, and fingerprint spoofing detection,” *IEEE Transactions on Information Forensics and Security*, vol. 10, no. 4, pp. 864–879, 2015.
- [35] T. Chugh and A. K. Jain, “Fingerprint spoof detector generalization,” *IEEE Transactions on Information Forensics and Security*, vol. 16, pp. 42–55, 2020.
- [36] Y. Zhang, D. Shi, X. Zhan, D. Cao, K. Zhu, and Z. Li, “Slim-rescnn: A deep residual convolutional neural network for fingerprint liveness detection,” *IEEE Access*, vol. 7, pp. 91 476–91 487, 2019.
- [37] R. R. Selvaraju, M. Cogswell, A. Das, R. Vedantam, D. Parikh, and D. Batra, “Grad-cam: Visual explanations from deep networks via gradient-based localization,” in *Proceedings of the IEEE international conference on computer vision*, 2017, pp. 618–626.
- [38] T. Brooks, B. Mildenhall, T. Xue, J. Chen, D. Sharlet, and J. T. Barron, “Unprocessing images for learned raw denoising,” in *Proceedings of the IEEE/CVF Conference on Computer Vision and Pattern Recognition*, 2019, pp. 11 036–11 045.
- [39] P. Perona and J. Malik, “Scale-space and edge detection using anisotropic diffusion,” *IEEE Transactions on pattern analysis and machine intelligence*, vol. 12, no. 7, pp. 629–639, 1990.
- [40] L. I. Rudin, S. Osher, and E. Fatemi, “Nonlinear total variation based noise removal algorithms,” *Physica D: nonlinear phenomena*, vol. 60, no. 1-4, pp. 259–268, 1992.
- [41] K. Zhang, W. Zuo, Y. Chen, D. Meng, and L. Zhang, “Beyond a gaussian denoiser: Residual learning of deep cnn for image denoising,” *IEEE transactions on image processing*, vol. 26, no. 7, pp. 3142–3155, 2017.
- [42] C. Xie, Y. Wu, L. v. d. Maaten, A. L. Yuille, and K. He, “Feature denoising for improving adversarial robustness,” in *Proceedings of the IEEE/CVF Conference on Computer Vision and Pattern Recognition*, 2019, pp. 501–509.
- [43] A. Vaswani, N. Shazeer, N. Parmar, J. Uszkoreit, L. Jones, A. N. Gomez, Ł. Kaiser, and I. Polosukhin, “Attention is all you need,” in *Advances in neural information processing systems*, 2017, pp. 5998–6008.
- [44] J. Hu, L. Shen, and G. Sun, “Squeeze-and-excitation networks,” in *Proceedings of the IEEE conference on computer vision and pattern recognition*, 2018, pp. 7132–7141.
- [45] J. Fu, J. Liu, H. Tian, Y. Li, Y. Bao, Z. Fang, and H. Lu, “Dual attention network for scene segmentation,” in *Proceedings of the IEEE/CVF Conference on Computer Vision and Pattern Recognition*, 2019, pp. 3146–3154.
- [46] S. Chaudhari, V. Mithal, G. Polatkan, and R. Ramanath, “An attentive survey of attention models,” *arXiv preprint arXiv:1904.02874*, 2019.
- [47] K. Xu, J. Ba, R. Kiros, K. Cho, A. Courville, R. Salakhudinov, R. Zemel, and Y. Bengio, “Show, attend and tell: Neural image caption generation with visual attention,” in *International conference on machine learning*. PMLR, 2015, pp. 2048–2057.
- [48] M. Sandler, A. Howard, M. Zhu, A. Zhmoginov, and L. C. Chen, “Mobilenetv2: Inverted residuals and linear bottlenecks,” *2018 IEEE/CVF Conference on Computer Vision and Pattern Recognition (CVPR)*, 2018.
- [49] T. DeVries and G. W. Taylor, “Improved regularization of convolutional neural networks with cutout,” *arXiv preprint arXiv:1708.04552*, 2017.
- [50] O. Russakovsky, J. Deng, H. Su, J. Krause, S. Satheesh, S. Ma, Z. Huang, A. Karpathy, A. Khosla, M. Bernstein *et al.*, “Imagenet large scale visual recognition challenge,” *International journal of computer vision*, vol. 115, no. 3, pp. 211–252, 2015.
- [51] R. Gajawada, A. Popli, T. Chugh, A. Namboodiri, and A. K. Jain, “Universal material translator: Towards spoof fingerprint generalization,” in *2019 International Conference on Biometrics (ICB)*, 2019, pp. 1–8.
- [52] X. Zhang, X. Zhou, M. Lin, and J. Sun, “Shufflenet: An extremely efficient convolutional neural network for mobile devices,” in *Proceedings of the IEEE conference on computer vision and pattern recognition*, 2018, pp. 6848–6856.
- [53] A. G. Howard, M. Zhu, B. Chen, D. Kalenichenko, W. Wang, T. Weyand, M. Andreetto, and H. Adam, “Mobilenets: Efficient convolutional neural networks for mobile vision applications,” *arXiv preprint arXiv:1704.04861*, 2017.
- [54] F. Chollet, “Xception: Deep learning with depthwise separable convolutions,” in *Proceedings of the IEEE conference on computer vision and pattern recognition*, 2017, pp. 1251–1258.
- [55] A. Paszke, S. Gross, S. Chintala, G. Chanan, E. Yang, Z. DeVito, Z. Lin, A. Desmaison, L. Antiga, and A. Lerer, “Automatic differentiation in pytorch,” 2017.